International Journal of Nanomedicine

Dovepress
open access to scientific and medical research

Open Access Full Text Article

ORIGINAL RESEARCH

α-Bisabolol-Loaded Cross-Linked Zein Nanofibrous 3D-Scaffolds For Accelerating Wound Healing And Tissue Regeneration In Rats

This article was published in the following Dove Press journal:
International Journal of Nanomedicine

Sarah A El-Lakany[1]
Ahmed I Abd-Elhamid[2]
Elbadawy A Kamoun[3,4]
Esmail M El-Fakharany[5]
Wael M Samy[1]
Nazik A Elgindy[1]

[1]Department of Industrial Pharmacy, Faculty of Pharmacy, Alexandria University, Alexandria, Egypt; [2]Nanotechnology and Composite Material Research Department, Advanced Technology and New Materials Research Institute, City of Scientific Research and Technological Applications (SRTA-City), Alexandria 21934, Egypt; [3]Polymeric Materials Research Department, Advanced Technology and New Materials Research Institute, City of Scientific Research and Technological Applications (SRTA-City), Alexandria 21934, Egypt; [4]Nanotechnology Research Center (NTRC), The British University in Egypt (BUE), El-Sherouk City, Cairo 11837, Egypt; [5]Therapeutic and Protective Proteins Laboratory, Protein Research Department, Genetic Engineering and Biotechnology Research Institute, City of Scientific Research and Technological Applications (SRTA-City), Alexandria 21934, Egypt

Objectives: Novel α-bisabolol (BIS)-loaded citric acid cross-linked zein nanofibrous scaffolds (C-ZNFs) were proposed to serve as safe platforms for promoting wound repair in rats.
Methods: ZNFs were synthesized using electrospinning technique, then NFs, with adequate water resistance, were produced using citric acid as a safe cross-linker.
Results: Compared to the uncross-linked ZNFs, cross-linking with 7% w/w citric acid decreased swelling index by 3 folds, while the tensile strength and the contact angle were enhanced to 2.5 and 3.8 folds, respectively. SEM images showed beads-free homogeneous NFs with a fully inter-connected 3D-network, where the average diameter of optimized C-ZNFs was 181.7±50 nm. After 24 h, C-ZNFs exhibited a decreased BIS release rate (45.6%), compared to uncross-linked mats (84.9%). By increasing BIS concentration, the cell adhesion (WI38 fibroblasts) was improved which can be attributed mainly to BIS activation of transforming growth factor-beta (TGF-β1). The MTT-OD obtained values indicated that all tested zein scaffolds significantly enhanced the viability of WI38 fibroblasts, compared to the control after 48h of incubation which can be referred to the proliferative potential of zein by provoking cell spreading process. The scratch wound assay demonstrated that BIS-loaded ZNF scaffolds showed accelerated migration and proliferation of fibroblasts expressed by significantly higher wound closure rates compared to the control sample. BIS-loaded-C-ZNFs prominently accelerated tissue regeneration for wound closure demonstrated by entirely grown epithelium with normal keratinization and rapid wound contraction, compared to the control. Immunohistochemical results confirmed the superiority of BIS-loaded-C-ZNFs, where the observed reduced NF-κB and the elevated cytokeratin expressions confirmed the anti-inflammatory and proliferative effects of the scaffolds, respectively.
Conclusion: In-vitro, optimized C-ZNFs offered a satisfactory cytocompatibility, adhesion and healing which were consistent with the in-vivo results. BIS-loaded-C-ZNFs could be regarded as a promising and effective biomaterial for tissue regeneration and for accelerating the wound healing process.

Keywords: cell compatibility, electrospinning, German chamomile, fiber mats

Introduction

The incidence of acute and/or chronic wounds represents health and economic burdens.[1] Skin wounds may originate from surgical procedures, decubital ulcers, trauma, impaired circulations or burns. Normally, skin wound healing occurs through several consecutive overlapping phases of hemostasis, inflammation, proliferation, and remodeling.[2] Numerous factors might interfere with the phases leading to impaired wound healing which may necessitate the use of skin

Correspondence: Sarah A El-Lakany
Department of Industrial Pharmacy
Faculty of Pharmacy, Alexandria University, 1 El Khartoum Square, PO Box 21521, Alexandria, Egypt
Tel +20 3 1002828663
Fax +20 3 4871668
Email sarah.ellakany@alexu.edu.eg

submit your manuscript | www.dovepress.com
DovePress
http://doi.org/10.2147/IJN.S224315

substitutes with their accompanying risks. The use of xenografts, allografts or autografts for wound healing has been limited due to their antigenicity, retarded healing, risk of infection, or restriction of the donor site.[3] An encouraging alternative approach is tissue engineering with a broad range of applications in the treatment of lost organs. Nano-science studies are constantly offering promising alternative biomedical approaches such as 3D-structured nanofiber (NF) scaffolds that can be tailored to resemble the extracellular matrix (ECM). Such architecture may function as a physical sustenance for normal cell development, proliferation, differentiation and motility to boost the healing process.[4] Ideally, such a scaffold must be biocompatible and biodegradable with a highly porous structure and a proper mechanical strength.[3] However, polymeric biomaterials have been used in medical applications, where only a few examples were found to be clinically successful. Synthetic polymers are always restricted to the diversity of chemical composition, non-degradable nature, or complications owing to their degradation products. For instance, poly (lactic-co-glycolic acid) co-polymer amplifies the tissue-inflammable response owing to acid hydrolysis. On the other hand, the application of natural polymers introduces several vital features, including biodegradability, biocompatibility, and biological stability; thus these are much superior to the synthetic ones.

Zein, a plant protein, is classified as a safe material by the US-FDA. Due to its hydrophobic characteristics, it is considered an attractive natural protein polymer that is widely utilized as a carrier for controlling the release of hydrophobic drugs.[5] Various anticancer drugs and herbs including curcumin,[6] quercetin,[7] daidzin,[8] exemestane/luteolin[9] and exemestane/resveratrol[10] were successfully encapsulated in zein NPs. Although the fabrication of fibers from the vast majority of protein polymers is somewhat problematic, due to their complex macromolecular structure, zein can be easily processed into fibrous forms.[4] Zein scaffolds were found to have high porosity, microbial attack resistance, porous-walled structure, antioxidant activity, and adequate biocompatibility.[11,12] However, the mechanical weakness and morphological stability of zein fibers in wet conditions represent key restrictions. For addressing these challenges, it was found that the incorporation of other polymers such as poly(ε-caprolactone) bio-composite scaffold,[13] or using chemical cross-linkers such as glutaraldehyde[14] or citric acid (CA), improved the mechanical strength of fabricated zein fibers. Jiang and Yang,[15] found that the cross-linked zein fibers could keep their ultrafine fibrous nature after immersion in PBS at 37 ±0.5°C for two weeks, upon using CA as a cross-linker. Electrospinning technique was used as an efficient NF-fabrication technique combining cost-effectiveness, versatility and easiness.[16] The produced polymer-based NFs possess numerous merits, e.g. a high surface area, tunable porosity, and a controlled drug releasing pattern which make them excellent candidates for various applications.[17]

α-Bisabolol (BIS), a natural monocyclic unsaturated sesquiterpene alcohol extracted from the flower of German chamomile, was used in various cosmetics formulations, mostly in moisturizers, lotions, and emulsions in concentrations ranging from 0.1 to 1 w/v %.[18] BIS, which is soluble in various organic solvents, has a highly lipophilic nature and poor aqueous solubility (72.9 µg/mL).[19] As a multi-target phytochemical, BIS was found to reveal several pharmacological activities including anti-inflammatory, anti-allergic, antibacterial, antiseptic, anti-fungal and antioxidant effects, making its usage in the treatment of skin wounds an excellent target.[18] The anti-inflammatory effect was monitored by the ability of BIS to constrain leukocyte migration and inhibit NF-κB pathway which down-regulate the lipo polysaccharide (LPS)-evoked expression of nitric oxide synthase and cycloxygenase-2 genes.[20]

In the current study, optimized and entirely natural materials-based scaffolds of CA cross-linked zein NFs encapsulating BIS were prepared by electrospinning as a potential platform to promote wound healing. CA was employed as a safe chemical cross-linker to provide good mechanical electrospun ZNFs with the proper water resistance vital to various biomedical applications. ZNFs scaffolds are expected to function as physical support to guide the differentiation and the proliferation of cells into the targeted wounded tissues and help in tissue regeneration. BIS was intended to ameliorate the healing process due to its biological activities. The optimized formula may extend the therapeutic potential of BIS by providing a controlled release pattern and increasing its bioavailability. To the best of our knowledge, we are the first to successfully load BIS into zein NF mats for wounded tissues to help in their regeneration. For the first time, in-vitro scratch wound assay, cell adhesion, cell viability and in-vivo experimental procedures of excision wounds were conducted, along with histopathological and immunohistochemical studies to confirm the superior role of BIS zein scaffolds in the improved healing process.

Materials And Methods

Materials

Zein (Z), α-bisabolol (BIS), N,N-Dimethylformamide (DMF), citric acid (CA), Dimethyl sulfoxide (DMSO), Dulbecco's modified eagle medium (DMEM), 3-(4,5-dimethyl-thiazol-2-yl)-2,5-diphenyltetrazolium bromide (MTT), bovine serum albumin (BSA), fetal bovine serum (FBS), 3,3′-Diaminobenzidine (DAB), WI38 cell line human, haematoxylin, eosin, Masson trichrome stain and Canada balsam were purchased from Sigma-Aldrich (St. Louis, MO, USA). RPMI-1640 medium was purchased from Lonza (New Jersey, USA). Cytokeratin cocktail AE1/AE3 (Clone AE1/AE3, Catalog No: BSB 5431) antibody was purchased from BIO-SB (CA, USA). NF-Kappa-B (NF-κB) p65 Rabbit monoclonal antibody (Catalog No: A1591) was purchased from BioVision, Inc. (San Francisco, USA). WI38 cell line was purchased from (VSVRI, Cairo, Egypt), passage number 60. Other reagents and chemicals were used in an analytical grade.

Animals

Male Sprague Dawley rats (220 ±25 g) were housed individually in a pathogen-free environment under standard conditions of light, humidity, and temperature. All procedures were done according to a protocol approved by the Animal Care and Use Committee of the Faculty of Pharmacy, Alexandria University, Egypt and in accordance with the regulations of the National Research Council's guide for the care and use of laboratory animals.

Optimization Of Electrospun Zein NFs

Zein was dissolved in DMF at different concentrations ranging from 15 to 50% (w/v) with or without CA as a cross-linker (0, 1, 3, 5 and 7%, w/w). The prepared solutions were then electrospun into NFs at different voltages and different syringe-collector distances as shown in Table S1 and Table 1.

Electrospinning Of Optimized BIS-Loaded Citric Acid Cross-Linked Zein Nanofibrous Scaffolds (C-ZNFs)

Zein (50% w/v) was dissolved in DMF solution and was kept under stirring for 2 h at room temperature. The formed zein solution was then moved to a polypropylene plastic syringe with a 23G stainless steel blunt needle. Afterwards, the solution was electrospun at a voltage of 24 kV from a high voltage source (Gamma high voltage research, Inc., FL, USA) and the formed NFs were collected over a static plate collector kept at 26 cm from the needle, where the feeding solution rate was kept at 0.15 mL/h. To prepare CA cross-linked zein scaffolds (F12), CA (7%, w/w) was first added to the zein-DMF solution and incubated for 30 mins under stirring before electrospinning following the above-mentioned procedure. To fabricate drug-loaded C-ZNFs, BIS in amounts of (12.5, 25 or 50%w/w), based on the dry polymer weight, was dissolved in the CA/zein solution just before electrospinning and the NFs were obtained at the same spinning conditions. The scaffolds were collected on sheets of aluminum foil, dried under vacuum overnight to eliminate the residual DMF and kept in a dry/cold condition to prevent any possible contamination. The scaffolds were also collected on 15mm coverslips to carry out in-vitro experiments. All electrospinning experiments were performed at room temperature with relative humidity of 55%. The scaffolds were fabricated under aseptic condition.

Instrumental Characterizations Of BIS-Loaded C-ZNFs Scaffolds

The morphology of NF mats was investigated by SEM (SEM, Joel GSM-6610LV, Japan). Average fiber diameters and mean pore area were calculated by taking 100 readings from random NFs of each sample image analysis using the mixed segmentation algorithm of Diameter-J of Fiji 1.51s and (Image J, version 1.4.3) software.[21]

Tensile strength of ZNFs scaffolds in the dry state was measured by standard uniaxial tensile test (Z050, Zwick Roell AG, Ulm, Germany). The NFs were cut into rectangular pieces with dimensions (40×10 mm) and incorporated into paper frames to protect them before the definite tensile testing. To obtain the stress-strain curves, specimens were elongated at a speed of 10 mm/min with an initial length of 20 mm and 50N cell load. Measurements were taken for at least six specimens of each composition to obtain average values and standard deviations.

The chemical composition of C-ZNFs was analyzed by FTIR (IR, 8400s Shimadzu, Japan) with the IR fingerprints recorded between 4000–400 cm^{-1}.

Also, thermal degradation of blank ZNF mats and BIS/ZNFs was performed by thermogravimetric analysis (TGA) (TGA-50, Shimadzu, Japan). The dried samples were operated under nitrogen gas at a heating rate of 10 °C/min at a temperature range of 0–500 °C.

Physicochemical Characterizations Of BIS-Loaded C-ZNFs Scaffolds

Water Contact Angle

The surface wet-ability of zein scaffolds was determined by static water contact angle measurement using a contact angle goniometry (DSA30, Krüss GmbH, Hamburg, Germany). The scaffold samples were fixed onto microscope glass-slides then a deionized water droplet (30 µL) was dropped onto the scaffold surface at room temperature. The data was collected by DSA image analysis software (DSA4.2.0. Krüss GmbH, Hamburg, Germany).

Moisture Uptake

A precisely weighed specimen (9 cm^2) of zein–based NF scaffolds was placed on a petri-dish in a desiccator filled with water. After 24h, the mats were re-weighed to calculate the moisture uptake percentage using the following equation:

$$\text{Moisture uptake } (\%) = (W_s - W_0)/W_0 \times 100 \quad (1)$$

Where W_s is the weight of the swollen NF, and W_0 is the weight of the original NF.

Swelling Index

Zein–based NF scaffolds were weighed individually (W_1) and immersed separately in a petri-dish containing PBS, pH 6.8. After 5 mins, samples were detached and the excess water was dried by a fine towel paper. The swollen films were re-weighed (W_2) at intervals against the change of sample weight, as given in equation 2.

$$SI = (W_2 - W_1)/W_1 \quad (2)$$

Drug Payload And In-Vitro BIS Release Study

To determine BIS content, 100 mg BIS-loaded C-ZNFs were weighed and treated with 10 mL DMF under sonication for 5 min. The solution was then filtered through a 0.22 µm membrane filter, diluted with DMF and the BIS content was assayed at 241 nm using UV–Vis spectrophotometer (UV-2102PC, Unico Instrument Co. Ltd., Shanghai, China).[22,23] The drug loading efficiency (LE %) was determined using the given equation.

$$LE\,\% = (\text{amount of BIS in scaffold})/(\text{amount of scaffold taken}) \times 100 \quad (3b)$$

For measuring the BIS release from C/ZNFs, 100 mg of BIS drug-loaded mats were placed on a plastic support of the same area, covered with a pre-soaked cellulose ester dialysis bag (12–14 kDa MWCO Visking dialysis tubing, SERVA, Germany) and the whole set was fully immersed in 50 mL of PBS and kept in a shaker incubator (50 rpm, at 37 °C). At appointed intervals, 3 mL of the release medium was extracted and replaced with the same volume of the drug-free medium. BIS in the samples were measured spectrometrically at 241 nm. For analyzing the kinetic model of BIS release from the developed zein scaffold, the obtained release results were fitted into zero-order, first-order and Higuchi equations. The release data were subjected to kinetic analysis using the *Korsmeyer–Peppas* model correlating drug release to time by the simple exponential equation for the fraction of drug release.[24]

Bio-Evaluation Tests

In-Vitro Cell Adhesion Analysis

Blank 7% w/w C-ZNF (F12) mats, and their corresponding BIS-loaded (F13, F14 and F15) ones, collected on glass coverslips, were placed in a 24-well plate prior to cell seeding. Plain coverslips were treated as controls. Human normal WI38 cells (2.0 $\times 10^5$) were seeded into the 24-well plate in RPMI-1640 media supplemented with (10% w/v FBS at 37°C for 0.5, 2, 4 and 6h). After the incubation period, the wells were washed gently with warm phosphate-buffered saline (PBS) to remove the non-adherent cells. The number of attached cells was determined by adding 100µL/well of 0.1 (w/v, %) crystal violet solution and incubated at room temperature for one hour. Then, the cells were washed thrice with 1.0M PBS and the absorbance was measured through spectrophotometry with a micro-plate-reader at 570nm.

In-Vitro Cell Viability Of C-ZNFs Scaffolds

The effect of the selected blank C-ZNF scaffold (F12) and its BIS-loaded C-ZNFs with (F13, F14 and F15) on the viability of WI38 normal cells, were assayed using the MTT assay following the earlier mentioned protocols by Al-Mahdy et al[25] and Mosmann.[26] In brief, human normal WI38 cells (2.0 $\times 10^5$) were seeded in 96-well bottom tissue culture plates and cultured in RPMI-1640 medium supplemented with (10% w/v FBS at 37°C in 5% CO_2) incubated to become about 80% confluent. Then, tested samples (50 µM) were added to the cells in triplicates for 48h. After incubation at 37 °C in a 5% CO_2 incubator, the cells were washed three times with fresh media and 200 µL of MTT solution (0.5 mg/mL) was added to each well and incubated at 37 °C and 5% CO_2 for 24h. The formazan crystals were dissolved in 100µL/well of DMSO

and the absorbance or OD was assessed through spectrophotometry with a micro-plate reader at 570 nm. The obtained results were represented graphically as (%) viability versus concentrations by the Graphpad Prism 6 software. The relative cell viability (%) was calculated using Equation 4 below.

$$\text{Cell viability } (\%) = (OD_s/OD_c)\times 100 \quad (4)$$

Where OD_s is the mean optical density of the sample and OD_c is the mean optical density of the control group.

In-Vitro Scratch Wound Assay

Human normal WI38 cells (2.0×10^5) were seeded in 12-well tissue culture plates and left overnight in 5% CO_2 incubated at 37°C. Once the cells reached a confluent monolayer, a scrape was carried out in a straight line with a pipette tip on the monolayer.[27] Cells were double washed with PBS to eliminate cell debris. Afterward, the release medium of a blank C-ZNF scaffold (F12) and various BIS-loaded 7% w/w C-ZNFs (F13, F14, and F15) were immediately added to the wells and incubated under the abovementioned conditions to allow cell migration to the medium. The wound healing was evaluated after one and two days using a phase-contrast microscope in comparison with the control cells.

In-Vivo Experimental Procedures Of Excision Wounds

Animals were anesthetized by intraperitoneal injection of 3% w/v pentobarbital sodium solution (1mg/kg), during the whole surgical procedures.[28] The dorsal area of the skin of the rats was shaved with an electric animal clipper (Wahl professional animal Deluxe U-Clip Pet Clipper, USA). The skin was primed by scrubbing it with cetrimide-chlorhexidine (1:30) solution followed by ethanol (70%). Circular full-thickness skin wounds (1.7 cm^2) were excised from the dorsum of each rat.[29] To investigate the in-vivo wound healing efficiency of drug-loaded zein scaffolds, animals were randomly assigned to four groups (12 rats each). The groups included untreated positive control, free BIS, F12 (blank ZNF scaffold) and F15 (BIS-loaded C-ZNFs scaffold) treated groups. Free drug or scaffolds, equivalent to 3 mg BIS, were applied once topically. Wounds were covered with gauze and a porous 3M Micropore™ adhesive tape after application to secure the scaffolds in place. A total of 48 rats underwent such procedures, where on days 3, 6, 9 and 14 post-wounding, two rats were taken from each group for histological and immune-histochemical analysis by full-thickness skin excision of the wound area.

Wound Contraction Rate/wound Healing Performance

This test is monitored for the most prominent changes commonly occurring during the wound healing process. Thus, every 3 days till day 14, the wound area was photographed and the wound contraction was evaluated by measuring the wound zone calculated as % reduction in wound zone compared to the original wound zone at zero time.

Histological Study

For histological analysis, samples from the wound edge were fixed in 4% v/v formaldehyde/PBS solution, then dehydrated with a graded run of ethanol, embedded in paraffin, and sectioned. Haematoxylin and eosin (H&E) and Masson's trichrome stainings were performed on various wound sections, and biopsies were observed under an optical microscope for epithelialization, and keratinization investigation. Nine random fields (n=9) of three stained sections of each group were blindly investigated from healing zones at *40. Stained sections were scored on a 0–4 numerical scale for the inflammatory infiltrates, as described earlier.[30] The scores were 0 for absence, 1 for occasional presence, 2 for light scattering, 3 for abundance, and 4 for the confluence of cells. The epithelization was graded from 0–3 as per the method of Abramov et al,[31] and the scoring was 0 for none, 1 for partial, 2 for the complete, but immature or thin, and 3 for complete and mature epithelial layer. The staining intensity of the collagen fibers with Masson trichrome was graded under ×40 magnification as follows: 1= completely negative staining intensity; 2= lower staining intensity; 3= moderate staining intensity; 4= slightly higher staining intensity; 5= considerably higher staining intensity.[29]

Immunohistochemical Analysis

For immunohistochemical analysis, wound beds, collected at 3, 6, 9 and 14 days post-treatment, were fixed with 10% v/v formaldehyde solution for 24h then, embedded in paraffin blocks. For the staining process, a 3 μm section of each block was positioned on positively charged microscope slides, de-paraffinized by being washed three times in xylene and rehydrated in different ethanol concentrations. The slides were left to boil in a 0.01M citrate buffer and heated in a microwave for antigen retrieval.[32] Then, primary antibodies, including pancytokeratin AE1/AE3 or

NF-κB, were added after being diluted at 1:200. Secondary antibodies conjugated with horseradish peroxidase were incubated with the slides for 30 min., followed by the addition of diluted DAB chromogen. As a measure of the protein expression, the immunohistochemical signals of pancytokeratin AE1/AE3 and NF-κB were quantified by the use of Image-J software (version 1.4.5s) together with computer-assisted microscopy.

Statistical Analysis

All measurements were carried out at least in triplicate and quantitative data were analyzed with (SPSS version 16.0, USA), and were presented as a mean± standard deviation. Significant differences between specimens were evaluated using (ANOVA) and Turkey's Multiple. The difference was considered significant when p values < 0.05.

Results And Discussion

Optimization Of Uncross-Linked ZNFs Scaffolds

The details of optimization were conducted to prepare morphologically accepted zein NFs without droplets formation, where the effects of zein concentration (30, 40 and 50% w/w), feeding rate (0.15–2.0 mL/h), voltage (18 and 24 kV) and tip-to-target distance (14, 20 and 26 cm) on zein NFs morphology, diameter and average pore size were studied and are shown in Tables 1, 2 and S1 (supplementary material).

Morphology Of ZNFs Scaffolds

SEM images showed the morphology of the selected fabricated zein scaffolds which are demonstrated in Figure 1. The average diameters of all NFs, investigated using the mixed segmentation algorithm of Diameter-J of Fiji 1.51s and (Image J, version 1.4.3) software, ranged from 160.1 ±39 to 281.2±65 nm (Table 2 and Figure 1). The images show that only irregular spherical beaded structures were formed at low zein concentration (F7; 30%, w/v), which can be attributed to the low viscosity of the polymer solution. However, increasing the zein concentration solution to 40%, w/v (F8), produced NFs with a diameter of (~167.9±85 nm) and a significantly reduced number of formed beads. Following previous studies, the optimized uncross-linked zein scaffold (F2) was achieved when 50% (w/v) zein solution was employed.[33] This phenomenon is common for the electrospinning of various polymeric solutions, where high polymer concentrations allow the alteration from bead particles to a bead-free NFs. Since increasing zein concentration leads to increasing the solution viscosity, more polymer chain entanglements were established. Thus, the electrified polymer jet can be fully stretched eradicating the beaded structure in the produced NFs.[33] Deitzel et al,[34] revealed that the formation of bead-free electrospun membrane of polyethylene oxide depends

Table 1 Optimization Of Spinning Conditions Of ZNF Scaffolds (mean ± SD, N =3)

Sample Code	Voltage (kV)	Feeding Rate (mL/h)	Tip To Target Distance (cm)	Zein Concentration (%, w/v)	CA Concentration (%, w/w)	BIS (%, w/w) Per Solid Polymer	Fiber Morphology Observation
F1	18	0.15	26	50	0	0	Ribbon-like NFs
F2	24	0.15	26	50	0	0	Beads-free NFs
F3	24	0.25	26	50	0	0	Ribbon-like NFs
F4	24	0.35	26	50	0	0	Beads only
F5	24	0.15	14	50	0	0	Beads-free NFs
F6	24	0.15	20	50	0	0	Beads-free NFs
F7	24	0.15	26	30	0	0	No fibers formed
F8	24	0.15	26	40	0	0	Fibers with beads
F9	24	0.15	26	50	1	0	Beads-free NFs
F10	24	0.15	26	50	3	0	Beads-free NFs
F11	24	0.15	26	50	5	0	Beads-free NFs
F12	24	0.15	26	50	7	0	Beads-free NFs
F13	24	0.15	26	50	7	12.5	Beads-free NFs
F14	24	0.15	26	50	7	25	Beads-free NFs
F15	24	0.15	26	50	7	50	Beads-free NFs
F16	24	0.15	26	50	0	50	Beads-free NFs

Table 2 Average Nanofiber Diameter, Diameter Skewness And Kurtosis, Pore Area And Mechanical Properties Of The Distinct Nanofiber Mats

Sample Code	Average Fiber Diameter (nm) ±SD	Diameter		Mean Pores Area (μm^2) ±SD	Tensile Strength (MPa) ±SD
		Skewness	Kurtosis		
F1	188.4±47	0.4961	0.4805	0.0937±1.3	–
F2	160.1±39	0.1106	0.4241	0.0915±1.2	1.49±0.27
F3	242.5±53	0.791	1.3462	0.0651±1.0	–
F4	281.2±65	0.5795	0.7051	0.0554±0.8	–
F5	175.1±66	1.138	2.7892	0.0288±0.3	–
F6	169.9±72	0.5233	0.2046	0.0307±0.4	–
F7	–	–	–	–	–
F8	167.9±85	1.6156	5.8039	0.0708±0.2	–
F9	173.2±48	1.1328	0.6917	0.0427±0.1	1.96±0.23
F10	183.7±68	0.5135	0.7543	0.0496±0.9	2.54±0.17
F11	181.8±50	0.2308	0.8644	0.0349±0.4	3.06±0.38
F12	179.2±25	0.1751	0.5974	0.0781±0.5	3.72±0.34
F13	173.7±24	0.1659	0.4872	0.0545±0.4	3.68±0.32
F14	158.1±33	0.3452	0.2457	0.0625±0.7	3.53±0.19
F15	127.6±59	0.1576	0.1779	0.0901±0.4	3.71±0.28
F16	132.5±38	0.4587	0.5078	0.0757±0.2	–

on the solution viscosity, where a viscosity above 1 Pa.s was required to produce a stable polymer jet.

Another studied factor affecting mat morphology was the influence of the electrospinning voltage which is represented in Figure 1 (F1 and F2). In accordance to Jiang et al,[33] increasing the spinning voltage from 18kV (F1) to 24 kV (F2), significantly diminished the formation of beads and changed the surface morphology from a ribbon-like shape to round NFs. When the feed rate was increased from 0.15 to 0.35 mL/h, the jet of zein solution was more likely to form beads (Figure 1; F2-F4). Such a result can be attributed to the increase in the size of the droplet formed and the destabilization of the Taylor cone during the electrospinning process.[35] Varying the distances between the tips of a spinneret to target did not affect the diameter of the obtained NFs. However, increasing the distance between the tip and the target diminished the bead formation (Table 1). Formulation F2 revealed bead-free round-shaped fibers with smooth surfaces and an average diameter of 160.1±39 nm. The diameter skewness and kurtosis of F2 were found to be 0.1106 and 0.4241, respectively, suggesting a symmetric normal distribution of the obtained results.[36] Also, F2 showed a mean pore area of 0.9153±1.2 μm^2 and a high density of pores formed in the scaffold network which can be attributed to the entanglement of the NFs.[37]

To prepare cross-linked C-ZNFs scaffolds, zein is allowed to react with CA (1, 3, 5 and 7% w/w) in DMF before electrospinning. The cross-linking mechanism of zein and CA has been previously discussed,[38] where amido-linkages between $-NH_2$ functional groups on the peptide chains of zein and the -COOH groups of CA are formed. The average diameters of C-ZNFs scaffolds (Table 2, F9–F12) ranged from (173.2±48 to 183.7±68 nm). These findings were insignificantly different from the uncross-linked zein scaffolds (Table 2, F2) in either diameters (160.1±39 nm) or morphology (Figure 1). For loaded scaffolds, BIS, an oily liquid, was perfectly miscible with a zein-DMF solution which prevented the incidence of phase separation leading to the formation of bead-free NF scaffolds with smooth surfaces (Figure 1; F15).[39] As shown in Table 2, raising the amount of BIS-loaded from 12.5 to 50% w/w (F13–F15) induced a prominent decrease in the obtained average diameter from 173.7±24 to 127.6±59 nm, which might be explained by a reduction in the solution viscosity.[40] A parallel behavior was observed by Lee et al,[41] where the addition of tannins into zein NFs shifted the diameter to less than 100 nm. These findings were attributed to the ability of tannins to decrease the viscosity which produced changes in the Taylor Cone tip and thus, affected the electrospinning process.[41] BIS-loaded uncross-linked ZNFs (F16) showed similar morphology and an insignificantly different diameter value (132.5±38 nm) compared to the cross-linked F15 mats (Table 2).

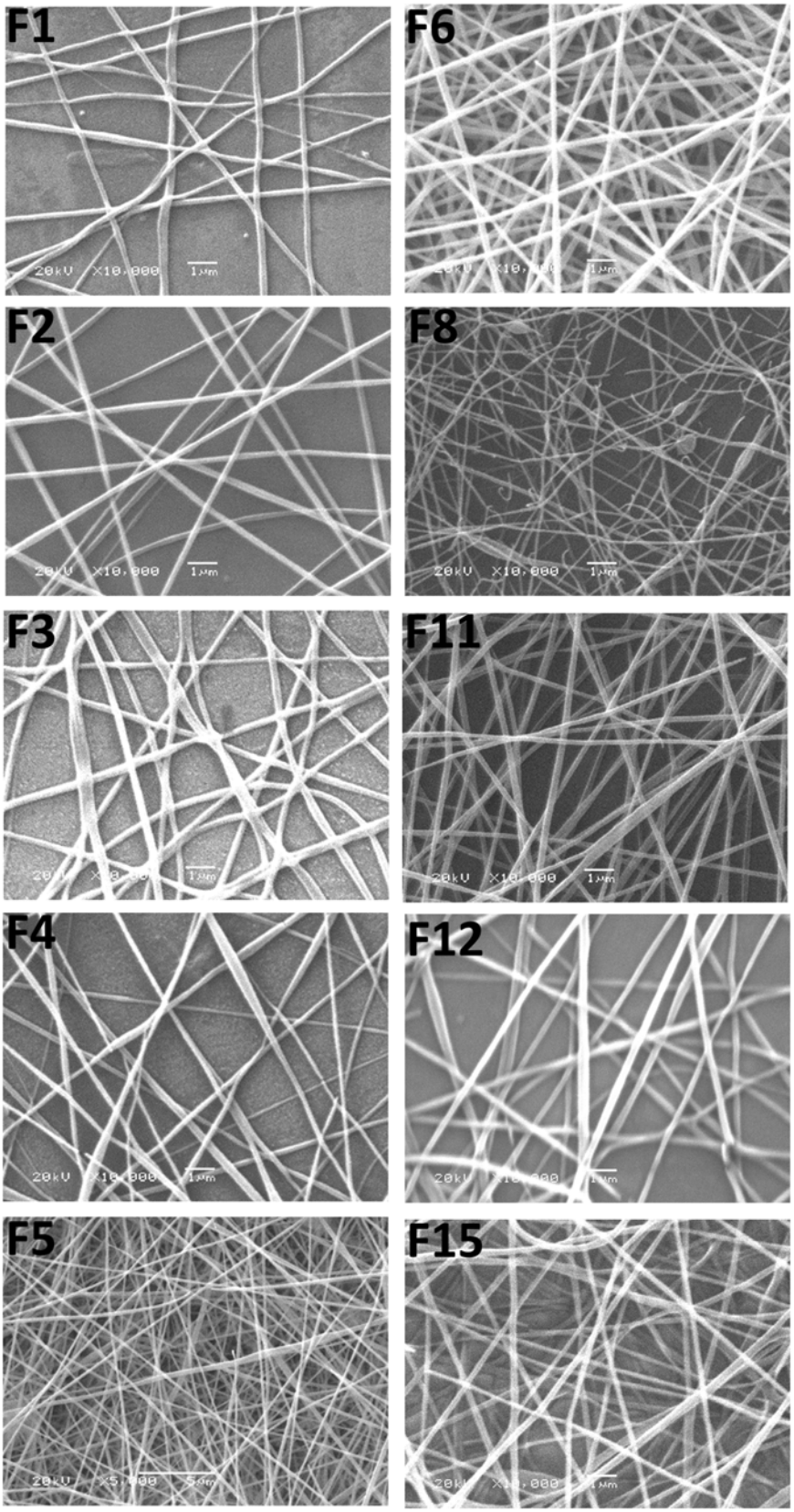

Figure 1 SEM images of selected zein nanofibrous scaffolds (according to Table 1); uncross-linked (F1–F6 and F8), cross-linked C-ZNFs (F11 and F12) and the optimized BIS-loaded 7% C-ZNFs (F15), (original magnification ×10,000). Scale bar is 1 μm.

Mechanical Properties Of ZNF Scaffolds

Uncross-linked ZNF scaffolds exhibited poor mechanical properties, as well as a very loose and flexible shape structure due to the lack of cross-linking. Using CA as cross-linker with different concentrations significantly promoted the mechanical properties of the mats, compared to uncross-linked ZNF scaffolds (Table 2). The scaffolds of F12 (7% w/w CA) exhibited the highest tensile strength of (3.72±0. 34 MPa), compared to the sample of F9 (1% w/w CA), F10 (3% w/w CA) and F11 (5% w/w CA) which exhibited a tensile strength of (1.96±0.23, 2.54±0.17 and 3.06±0.38 MPa), respectively (Table 2). The data obtained from the uniaxial tensile testing can be explained by the formation of the amido-linkages between CA and zein, where the cross-linking process enhanced the inter-connective structure between molecules and thus decreased their slippage during tensile testing.[38,42] Zein cross-linked with hexamethylene diisocyanate was reported to enhance its mechanical properties massively, where NFs electrospun from a 40% w/v zein solution exhibited an elevated tensile strength of 4.239 MPa.[43] Khalil et al,[42] found that zein cross-linked with 9% w/w CA offered a high tensile strength of 4.02 ± 0.37 MPa, while further increase of CA concentration reduced the mechanical strength. Other reports demonstrated the relation between the concentration of CA and the tensile strength of mats, where the increase of CA concentration up to 9% w/w augmented the available CA molecules for cross-linking portions, which improved the tensile strength; where higher concentrations triggered hyper-crosslinking resulting in diminished tensile strength.[44]

Chemical Structure Determination By FTIR

FTIR spectra of zein powder and F2 (uncross-linked blank ZNF scaffold) revealed characteristic protein peaks at 1249, 1531, and 1658 cm^{-1} related to the axial deformation vibrations of the C-N bond, angular deformation vibrations of the N-H bond of amide II, and stretching of the carbonyl (C=O) of amide I belonging to the peptide groups of zein, respectively (Figure 2A).[45,46] The spectra also showed a band between 2800 and 3500 cm^{-1} corresponding to the stretching of the N-H and O-H groups of the amino acids of the protein.[45] The spectrum of CA revealed its characteristic peaks at 1747 and 1702 cm^{-1} corresponding to the vibration peak of C=O bond of aliphatic carboxylic acid.[47] In concordance to Tavakolipour et al,[48] the IR spectra of all C-ZNFs scaffolds exhibited the appearance of a characteristic peak at 1670 cm^{-1} corresponding to carboxyl and ester carbonyl groups which ensure the formation of chemical linkages between zein and CA. The transmittance of the bands between 1658–1531 cm^{-1} of blank C-ZNFs scaffolds (F9–F12) was significantly reduced compared to pure zein, which confirmed the de-amidation of glutamine and the diminishment of the α-helical structure of zein.[48] While BIS showed its typical bands correlated to stretching of –OH between 3429–3300 cm^{-1} and characteristic peaks related to axial deformations of the C–H bonds between 3000–2890 cm^{-1}.[49] It was noticed that most of the absorption peaks of BIS, which exist in the IR spectra of BIS-loaded C-ZNFs scaffold (F15), offered lower intensities. The spectrum also presented the absorption stretching peak correlating to phenolic -OH groups of BIS shifted to 3298–3070 cm^{-1}, suggesting the possible formation of hydrogen bonds between BIS and CA cross-linked zein NFs.

Thermal Stability Of ZNF Scaffolds By TGA

TGA analysis was done to analyze the effect of cross-linker concentration in mats on thermal degradation of C-ZNFs scaffolds. The TGA graphs of all zein scaffolds have been displayed in Figure 2B, while the data were summarized and listed in Table 3. It was shown that the 1st degradation stage in the graph showed a higher moisture absorption in all samples of C-ZNFs scaffolds (F9–F12) compared to the original uncross-linked zein NFs (F2) because of the removal of moisture in ZNFs mats (≤ 100 °C). The 2nd degradation stage of graphs demonstrates that the thermal degradation onset (T_{onst}) and the temperature at 50% weight loss have increased progressively for F2 and F12 (248 to 268 °C and 375 to 430 °C, respectively) (Table 3). The incorporation of BIS into C-ZNFs mats (F15) showed a slight decrease in the thermal stability of C-ZNFs mats. As the content of CA increased in zein mats, the residue was also increased to thermally decompose in the 3rd stage which provides higher thermally stable mats, due to the effect of cross-linking by CA.

Wettability Measurement

Since the degree of wettability greatly affects protein adsorption and cell adhesion of the material, the value of the contact angle gives insight into the degree of wetting upon the interaction between the material and a liquid.[50] Small contact angles (≤90°) correspond to the high hydrophilic surface, while large contact angles (90°-150°) correspond to low hydrophilic surface which is close to the

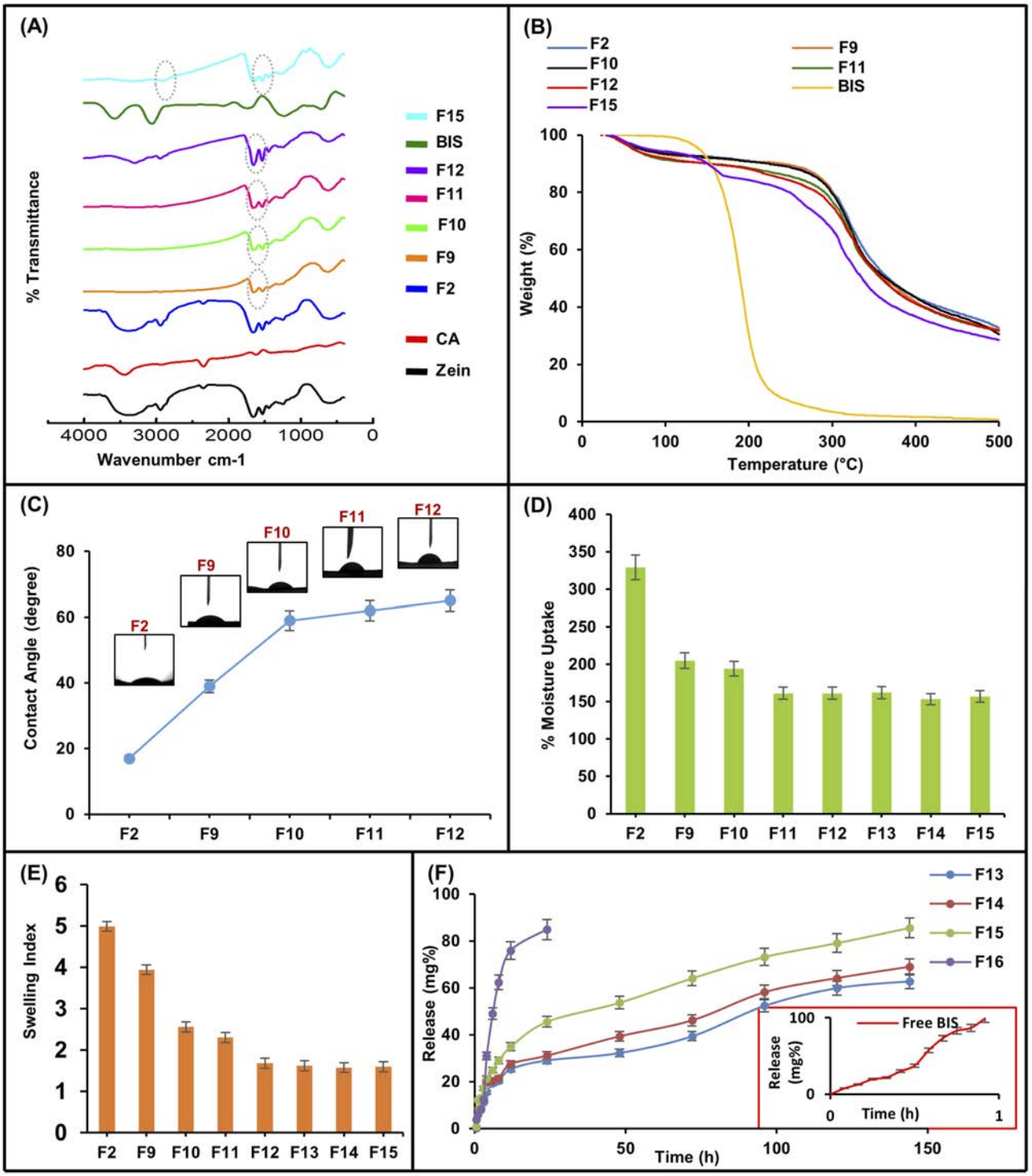

Figure 2 (**A**) FTIR spectra of zein, CA, BIS and selected ZNFs (F2, F9–F12 and F15), (**B**) TGA thermograph curves of selected cross-linked C-ZNFs and BIS, (**C**) contact angle measurements of uncross-linked (F2) and (1–7%) cross-linked C-ZNFs (F9–F12) scaffolds, (**D**) % moisture uptake, (**E**) swelling index for uncross-linked (F2), (1–7%) cross-linked C-ZNFs (F9–F12) and BIS-loaded 7% C-ZNFs (F13–F15) scaffolds, and (**F**) the influence of BIS concentrations on the in-vitro release of BIS from uncross-linked (F16) and 7% C-ZNFs (F13–F15) in (PBS, pH 6.8 containing 0.5% w/v SLS at 100 rpm and 37±0.5 °C).

hydrophobic one and >150° is corresponding to super-hydrophobic surface.[50] The water contact angles of uncross-linked (F2) and various C-ZNFs (F9–F12) scaffolds are demonstrated in Figure 2C. Although zein is regarded as a hydrophobic protein, F2 scaffolds showed significant hydrophilic characteristic to water droplets with a contact angle value of 17°.[9] This can be attributed to reducing the morphological stability of zein when it was

Table 3 Thermal Data Of Uncross-Linked And Cross-Linked ZNFs Adapted From TGA Thermographs

Sample code	Weight Loss %w/w At 100 °C	T_{onset} °C	50% Weight Loss Temp. (°C)	1st Decomposition Stage °C, (weight loss %)	2nd Decomposition Stage °C), (Weight Loss %)
F2	7%	248°C	375°C	100–210°C, (9%)	286–437°C, (52%)
F9	6%	265°C	411°C	100–262°C, (12%)	268–435°C, (52%)
F10	6%	260°C	421°C	100–248°C, (17%)	250–438°C, (44%)
F11	9%	270°C	431°C	100–252°C, (14%)	255–405°C, (45%)
F12	7%	268°C	430°C	100–252°C, (17%)	257–406°C, (43%)
BIS	3%	130°C	177°C	100–129°C, (3%)	133–233°C, (88%)
F15	6%	225°C	410°C	100–220°C, (16%)	225–415°C, (44%)

electrospun into NFs. This was consistent with the published findings of Vogt, et al,[51] where zein mats were easily wetted immediately after water dropping onto their surface. Although such a behavior favors cell attachment and proliferation, CA cross-linking of the scaffolds was adopted as a strategy to enhance the morphological stability and to prevent the loss of fibrous structure of scaffolds upon contact with water molecules. The water contact angle of the scaffolds increased with increasing CA concentration, where the water contact angles of samples F9, F10, F11, and F12 scaffolds were 39°, 59°, 62°, and 65°, respectively (Figure 2C). The contact angles in the CA cross-linked scaffolds increased with the corresponding relatively high wettability of the NFs.

Moisture Uptake And Swelling Index Of C-ZNFs Scaffolds

An efficient wound dressing must be capable of removing the exudates at the wound site. In this regard, the absorption capacity of uncross-linked ZNFs (F2), CA cross-linked ZNFs (F9–F12) and BIS-loaded 7% w/w C-ZNFs (F13–F15) scaffolds were studied using two different approaches: the moisture uptake[52] and a modified swelling index method.[53] For F2, the moisture uptake and swelling index values were 329% and 4.99, respectively, which promote the absorption of large amounts of wound exudates as a result of the spinning process (Figure 2D and E). However, uncross-linked zein mats were reported to extensively swell and disintegrate as they suffer from poor water resistance which necessitates the fiber modification by cross-linkage.[54]

Cross-linking with CA decreased the moisture uptake of zein mats where the % moisture uptake was 205.1±13, 194.0±24, 161.4±23 and 161.2±14 (Figure 2D and E), for 1% CA (F9), 3% CA (F10), 5% CA (F11) and 7% CA (F12), respectively. Similarly, swelling indices were reduced in the same order with F9, F10, F11 and F12 showing values of 3.94±0.15, 2.55±0.09, 2.30±0.11 and 1.68±0.23, respectively. Despite this decrease in the % moisture uptake and swelling index of zein mats, the obtained results suggested acceptable uptake capacity which favors the removal of wound exudates keeping a good water resistance. However, insignificant changes in the moisture uptake or swelling index results were noticed with different BIS-loaded 7% C-ZNFs scaffolds, compared to 7% C-ZNFs mats.

Drug Content And In-Vitro BIS Release Study Of C-ZNFs Scaffolds

Effective addressing of wound healing requires optimum drug loading along with sustaining and controlling the drug release profile at the desired site. To assess the efficiency of incorporating BIS into C-ZNFs scaffolds, % LE was measured. The % LE of F13 (12.5 % w/w loaded BIS), F14 (25% w/w loaded BIS) and F15 (50% w/w loaded BIS) were 9.5±32, 17.8±45 and 29.4±21%, respectively, which suggests successful loading of BIS into these scaffolds.

One of the characteristic features of electrospun mats is obtaining a sustained release profile of active components into the surrounding environment, by varying the selected polymer matrices and/or the processing parameters.[17] The key release mechanisms of a drug from the NF scaffolds belong to the diffusion from pores and desorption from the surface.[39] The in-vitro release pattern of BIS showed that the free drug presented a quick dissolution and reached about 100% of the dose after one hour, indicating that the cellulose membrane was not a limiting factor in the controlled release of BIS (Figure 2F). The incorporation of BIS into uncross-linked ZNFs (F16) resulted in a sustained drug release over 24 h. The cross-linking of zein scaffolds resulted in prolonging the release rate of BIS for up to 6 days with about 45.6 % of BIS released from F15 after 24 h, compared with 85% released from F16 over the same duration. It was noted that decreasing BIS to 12.5% w/w (F13) markedly decreased the rate of BIS release to reach 29% after 24h, compared to 32% and 46% released after the same duration from F14 (25% w/w loaded BIS) and F15 (50% w/w loaded BIS), respectively. The initial burst effect present in the release profiles of mats can be attributed to BIS desorption from the mat surface followed by diffusion from pores. The release kinetics of BIS from BIS-loaded C-ZNFs were investigated by fitting the in-vitro release data into mathematical models based on *zero-order, first-order, Higuchi kinetic, and Korsmeyer–Peppas* equations, and then calculating the correlation coefficient (R^2). As shown in Table 4, the fitting quality of the electrospun mats was achieved through the *Korsmeyer–Peppas* model. For BIS, the calculated values of n were <0.45 characterizing for the *Fickian*-diffusion mechanism.[24]

Cell Adhesion Evaluation Of C-ZNFs Scaffolds

The main feature of fibrous structures is the presence of micro/nanopores which contribute to the healing process. Such porous systems, resembling the ECM, provoke the cells to invade into the interior and boost oxygen and nutrients supply.[39] SEM data showed that ZNFs scaffolds had a high porosity structure, where the area of the pores ranged from 0.02883 to 0.0937 (μm^2) ±SD (Figure 1 and Table 2), which allows for excellent cell adhesion and proliferation. Moreover, zein itself was previously reported as a substrate for tissue transglutaminase which is an enzyme in cell-surface interactions by forming a bridge between integrin and fibronectin.[55] The bridging between zein and tissue transglutaminase offers a platform for effective cell adhesion. Figure 3A confirms the significant enhancement of cell adhesion onto all zein scaffolds, compared to the control sample, with the cell adhesion increase with increasing the amount loaded-BIS into C-ZNFs scaffolds. Increasing BIS concentration improved the cell adhesion which can be attributed to BIS activation of transforming growth factor-beta (TGF-β1), a multifunctional cytokine, in in-vitro cultured keratinocytes.[56] TGF-β promotes cellular adhesions by adjusting the expression of cadherin, a cell adhesion through the activation of focal adhesion kinase.[57]

In-Vitro Cell Viability Of C-ZNFs Scaffolds

MTT assay is a rapid and precise quantitative colorimetric dye-based assay that depends on the metabolic activity of viable cells, and is widely employed to determine cell growth and proliferation. The MTT-OD obtained values indicated that all tested zein scaffolds significantly enhanced the viability of WI38 fibroblasts, compared to the control (OD value =0.71) after 48h of incubation (Figure 3B). Moreover, all C-ZNF scaffolds loaded with 12.5, 25, and 50% w/w BIS (F13–F15) offered good cell viability compared to the control sample. This can be referred to the nano-topographic

Table 4 In-Vitro Release Kinetic Parameters For BIS From Different BIS-Loaded 7% C-ZNFs Formulations Using PBS pH 6.8; 0.5% (w/v) Of SLS At 37±0.5 °C

Nanofiber Code (%BIS)	*Zero-Order* Model		*First-Order* Model		*Higuchi* Model		*Korsmeyer-Peppas* Model		
	K_0 (% h^{-1})	R^2	K_1 (% $h^{-1/2}$)	R^2	K_H (% h^{-1})	R^2	K_{KP} (% h^{-n})	n	R^2
F13 (12.5%BIS)	0.387	0.9566	0.008	0.7741	5.342	0.9565	7.293	0.428	0.9686
F14 (25%BIS)	0.423	0.9166	0.010	0.7875	5.933	0.9644	8.387	0.420	0.9803
F15 (50%BIS)	0.524	0.8949	0.018	0.8285	7.620	0.9595	11.850	0.398	0.9892

Notes: K_0, K_1, K_H and K_{KP} are the release rate constants for zero-order, first-order, Higuchi and Korsmeyer-Peppas models, respectively, n, is the release exponent for Korsmeyer-Peppas model.

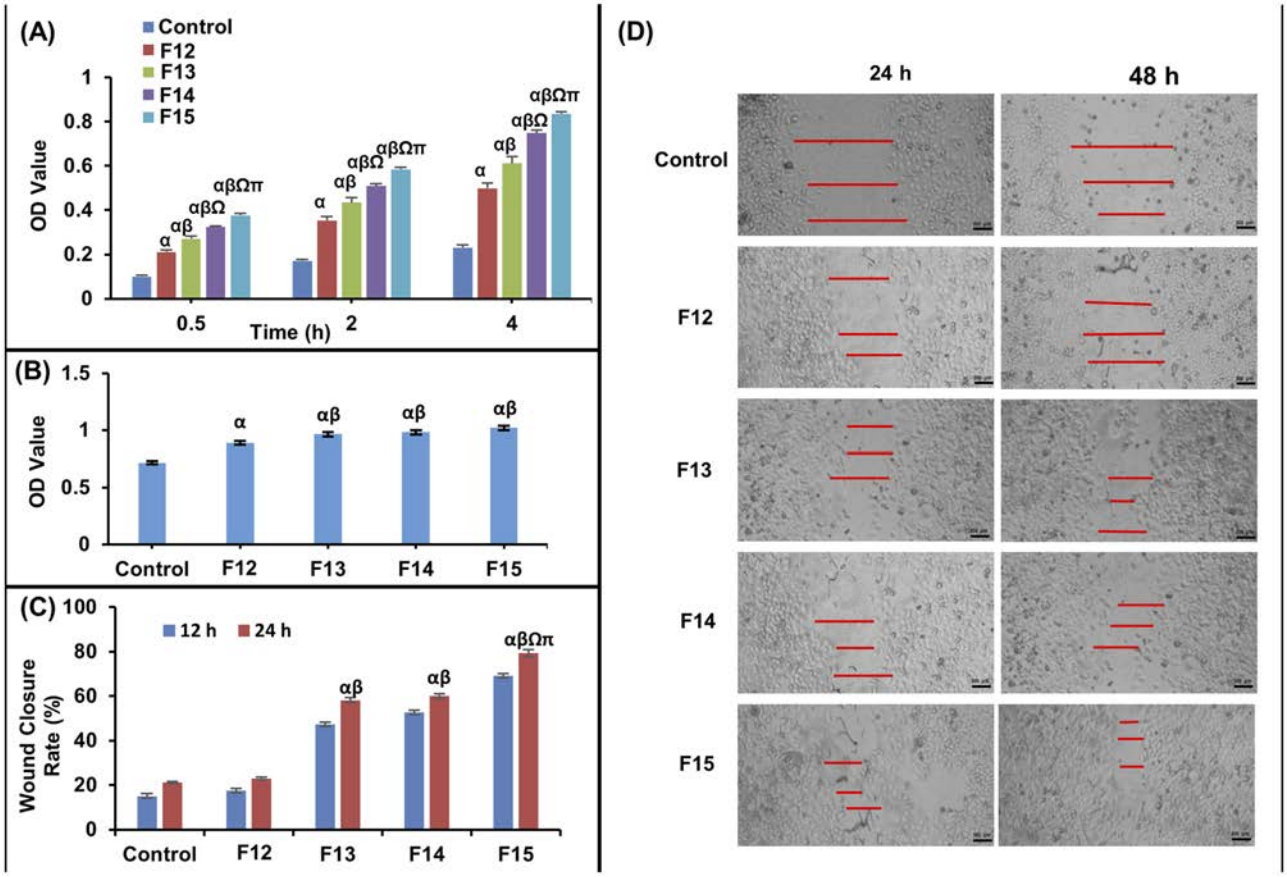

Figure 3 (**A**) Quantitative analysis of the cell adhesion potential of various zein scaffolds, (**B**) The influence of blank 7% C-ZNFs (F12) and BIS-loaded C-ZNFS (F13–F15) on human normal WI38 cells proliferation after 24 h. Effect of control, blank 7% C-ZNFs (F12) and various BIS-loaded 7% cross-linked C-ZNFs (F13–F15) on (**C**) the percentage of wound area recovered and (**D**) micrographs of cell migration of WI38 fibroblasts at 24 and 48h (Scale bar is 500 μm). The red bars indicate the measured distances used in calculating the % wound closure. *(α P < 0.05 vs Control; β P < 0.05 vs F12 (blank 7% C-ZNFs); Ω P < 0.05 vs F13 (12.5% BIS-loaded 7% C-ZNFs); π P < 0.05 vs F14 (25% BIS-loaded 7% C-ZNFs))*.

architecture of the developed scaffolds resembling the ECM which promotes the proliferation of the fibroblasts.[28] Moreover, zein offers additional potential advantages being reported as a cytocompatible protein with a good ability for the proliferation of both HL-7702 cells and NIH3T3 cells.[58] Besides its cell adhesive properties, the proliferative potential of zein can be explained by provoking cell spreading which is a key process, following cell adherence, towards successful cell proliferation and growth.[55]

Scratch Assay

For an effective healing process, fibroblasts must proliferate and migrate to the wound bed, during the proliferation process, where they secrete the ECM of the granulation tissue.[59] Fibroblasts promote collagen secretion, re-epithelialization and neo-angiogenesis.[60] In this regard, a scratch wound assay was employed using WI38 fibroblasts to evaluate the migration and the proliferation patterns in response to various applied treatments. WI38 cell line is a human lung fibroblast cells derived from a normal aborted female fetus of a 3-month-gestation. Compared to the control, the wells treated with F12 exhibited insignificantly different rates of wound contraction at 24 and 48h, as presented in (Figure. 3C and D). All BIS-loaded ZNF scaffolds (F13–F15) showed accelerated migration and proliferation of fibroblasts expressed by significantly higher wound closure rates at both 24h and 48h, compared to the control sample. The addition of BIS at concentrations of 12.5 and 25% (F13 and F14, respectively) dose-independently improved the cell migration in the same manner as shown in Figure 3C and D. Increasing BIS concentration to 50% (F15) gave rise to better cell migration (Figure. 3C and D).

Bezerra et al[61] have reported that BIS could have a significant effect on the activation of K+ATP channels, such an effect can enhance the cell migration at least partially. Recently, K^+ channels have been reported to be key parameters of epithelial repair via regulating the epithelial cell motility and hence, promoting the cell migration and proliferation.[62]

In-Vivo Wound Healing Performance

A robust inflammatory response mediates a healthy healing process devoid of infection.[63] However, current emerging studies suggest that the depletion of one or more of the inflammatory cell lineages would augment the healing process.[64] Thus, using an anti-inflammatory agent with antibacterial activity would evade unnecessary activation or infection leading to the a normal progress of the healing process. In this regard, BIS, as an inflammatory blocking treatment, was incorporated into ZNFs for boosting the repair of the wound.[20] Zein scaffolds were selected due to their prominent merits in-vivo where the resemblance to ECM accompanied by their high surface-area-to-volume ratio, semi-permeability, and the used biocompatible polymers aid massively the healing phase.

For estimating the wound healing ability of the optimized BIS-loaded C-ZNFs electrospun scaffolds (F15), the corresponding mats were applied to wound spots in the rat dorsum. Photographs of the microscopic appearance of wound repair covered with electrospun mats and the calculated mean wound contraction rate at intervals are displayed in Figure 4A and Table 5, respectively. By observing the wound area at definite intervals of time, the reduction in wound area was calculated. All rats survived throughout the post-operative period until sacrificed. As summarized in Table 5, the WC50 values of free BIS, F12 and F15-treated groups (7.9, 6.1 and 4.6 days, respectively) were lower than those observed in the control group (8.7 days). F15-treated groups showed the most prominent enhancement in the wound contraction rate compared to control, free BIS or F12 treated-groups with wound contraction percentages of 48.3±4.9, 61.1±1.9, 83.2±3.1 and 98.9±0.4% at 3, 6, 9 and 14 days post-wounding, respectively (Table 5).

A histological examination from in-vivo experiments provided an insight into the consequences of each treatment. F15-treated groups revealed an accelerated healing process where on the 3rd day post-wounding, profound granulation tissue with moderate inflammatory cells started to appear with mild new vessel formation (Figure 4B). On the 6th day, the granulation tissue area continued to grow and the marked formation of fibroblasts was observed. On the 9th day, compared to F12-treated groups, highly extensive fibrosis occurred as a sign of enhanced proliferation.[65] On the 14th day, a fully keratinized intact epithelium covered a small and a less dense area of scar tissue, compared to other groups. The scoring of various wound sections showed that the overall presence of inflammatory cells was significantly lower and the epithelization was significantly more in F15-treated groups compared to other groups (Figure 4C and D). Also, normally-oriented coarse collagen fibers, which were highly stained using Masson trichrome stain, were nearly observed (Figure 4E). This can be attributed to the inhibitory effect of BIS on collagenase activity which would promote the collagen biosynthesis at a molecular level.[66] The histological outcome in F12-treated groups showed similar findings to F15-treated groups with a slower healing progressing where marked inflammatory infiltrate appeared on the 3rd day post-wounding and continued profoundly till the 6th day. On the 14th day, a complete epithelium was covering the surface of the scar tissue (Figure 4B). Although the formed collagen fibers were mature, they were much finer compared to F15-treated groups (Figure 4E). It is worth mentioning that the collagen fibers from wounds of the control and the free BIS-treated groups had least staining intensity and were not mature. The granulation tissue area continued to appear along with the absence of dominant inflammatory cells and the presence of an incomplete intact epithelium which reveals the retardation in the healing process.

The mechanism by which BIS-loaded C-ZNFs (F15) may enhance the healing process was explored via studying their effect on the inflammation and proliferation of the wound using NF-κB and cytokeratin AE1/AE3 expressions, respectively, in the immunohistochemical study. NF-κB, a pro-inflammatory signaling pathway, is responsible for the expression of inflammatory cytokines and chemokines.[67] As presented in Figure 5A and B, the immunohistochemical results showed that F15-treated groups had a significantly lower % expression of NF-κB compared to the other groups on the 3rd and 6th days post-wounding. The % expression level of

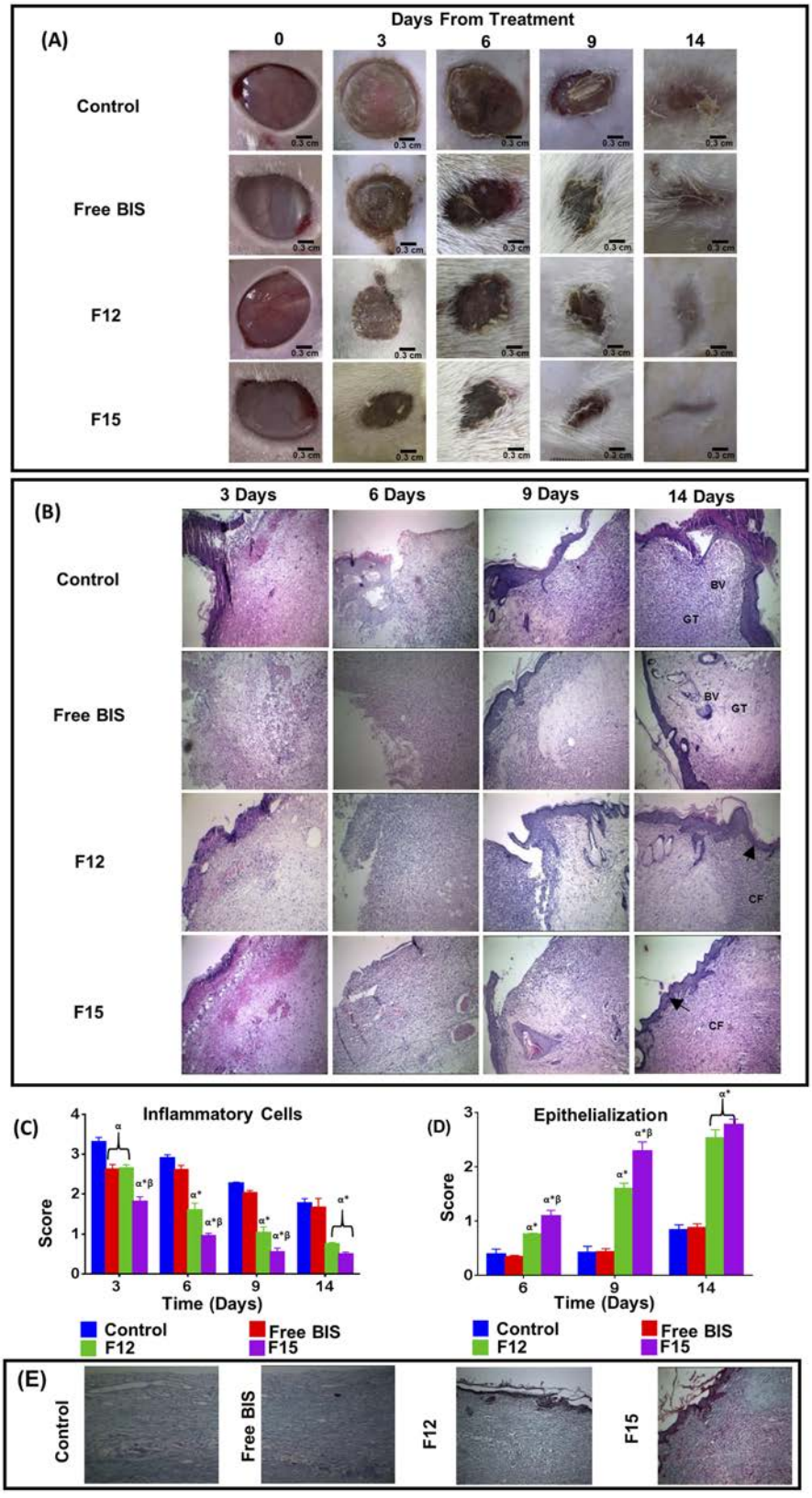

Figure 4 (**A**) Photographic images of in-vivo excision wound area contortion rate monitoring of control, free BIS, F12 (blank 7% C-ZNFs), and F15 (50% BIS-loaded 7% C-ZNFs scaffolds) *vs* day of contraction using dorsal of rats(Scale bar is 0.3 cm), (**B**) Representative images of H&E-stained histologic wound sections of control, free BIS, F12 and F15-treated groups on days 3, 6, 9, and 14 after wounding (The arrow indicates complete epithelisation. BV; blood vessel, GT; granulation tissue, CF; collagen fibers) (**C**) histologic scoring for inflammatory infiltrate (score from 0–4), (**D**) epithelisation (score from 0–3) from 9 randomly selected high-power fields (×40) from three H&E-stained cutaneous wound sections and (**E**) effect of different treatments on collagen fiber formation. *(α $P < 0.05$ vs Control; *$P < 0.05$ vs Free BIS; β $P < 0.05$ vs F12 (blank 7% C-ZNFs)).*

Table 5 Effect Of Free BIS, F12 (blank C-ZNFs) And F15 (50% BIS-Loaded 7% C-ZNFs) On Excision Wound Area Contraction And Half Closure Time (values Are Mean ± S.D., N =6 Observations In Each Group)

Day	Wound Contraction (%)			
	Control	Free BIS	F12	F15
3	15.9±2.3	27.3±7.2#	39.7±5.4#	48.3±4.9#
6	22.2±4.7	32.8±1.2#	47.3±6.6#	61.1±1.9#
9	51.5±1.9	59.2±5.6	71.4±2.4#	83.2±3.1#
14	83.1±0.9	90.7±0.5	95.2±0.7#	98.9±0.4#
WC_{50} (day)	8.7	7.9	6.1#	4.6#

Notes: Values are significant (#) at $P < 0.05$ as compared to the untreated group (control).
Abbreviation: WC_{50}, half closure time of wound contraction in days.

NF-κB declined dramatically by ~9 and 3 folds in F15-treated groups on the 9th and 14th days post-wounding, respectively, compared to the control. Such results can be explained by the sustained release of the anti-inflammatory drug, BIS, due to its ability to knock down NF-κB pathway which would down-regulate LPS-evoked expression of inducible nitric oxide synthase and cycloxygenase-2 genes. Thus, the inflammatory phase was terminated earlier in F15-treated groups and accelerated wound healing occurred. The relatively high NF-κB expression levels in BIS-treated groups can be explained by the insufficient treatment dosage where only a single application was applied.

The cytokeratin family includes keratins with varying molecular weights ranging from 40 to 70 kDa.[68] Cytokeratin is a cytoplasmic intermediate filament protein in the cytoskeleton of epithelial tissue produced via keratinocytes.[69] Following a skin insult, keratinocytes play a major role in cell migration, cell proliferation and reestablishment of the epidermal layer. Thus, the detection of keratins can be recognized as an early sign of normal maturation. Cytokeratin AE1/AE3 is a mix of monoclonal antibodies that can detect a wide spectrum of high and low molecular weight cytokeratin. Figure 5C and D show the immunohistochemical results of Cytokeratin AE1/AE3 in rats where the % expression of cytokeratin in F15-treated groups was higher compared to other groups on the 3rd, 6th, 9th and 14th days post-wounding. On day 3, F15-treated groups showed an overproduction of keratin demonstrated by the significantly highest % expression of cytokeratin (87.9±2.1%) compared to other groups which can be explained by the successful migration of keratinocytes from the basal layer to the surface of the wound epidermis layer.[69] Starting from about day 6, staining was lost from the basal cells and a scant brown stain started to appear on the most superficial layer as a sign of the proliferation of keratinocytes to rebuild the epidermis. The staining continued to increase in intensity and covered the wound on days 9 and 14 confirming re-epithelialization, keratinization and the restoration of skin functions. Sabol et al,[70] observed a similar pattern of cytokeratin production in the early stages of wound healing in a rat model. The control and BIS-treated groups showed a significant delay in the healing process, in terms of cell migration and epithelialization, compared to F15-treated groups. All these findings indicate the potential efficacy of loaded BIS onto C-ZNFs for accelerating wound healing and tissue regeneration.

Conclusion

In this paper, we have reported an efficient method of developing water-stable biocompatible 3D electrospun zein NFs by cross-linking with a safe cross-linker for biomedical applications. BIS as a natural wound healing promoter model was successfully incorporated into the fiber mats. The prepared C-ZNFs showed improved morphological and thermal stability in addition to an excellent swelling index and surface wettability. Wound healing in an animal model showed that zein mats generally improved wound contraction of 47% and 61% after 6 days for blank C-ZNFs (F12) and BIS-loaded C-ZNFs (F15) mat, respectively, compared with 22% for the control group. It was also noticed that loading of BIS onto C-ZNFs mats offered acceptable cell viability and sufficient cell adhesion. The results of this work demonstrated that BIS-loaded C-ZNFs scaffolds prepared by electrospinning could be used as a

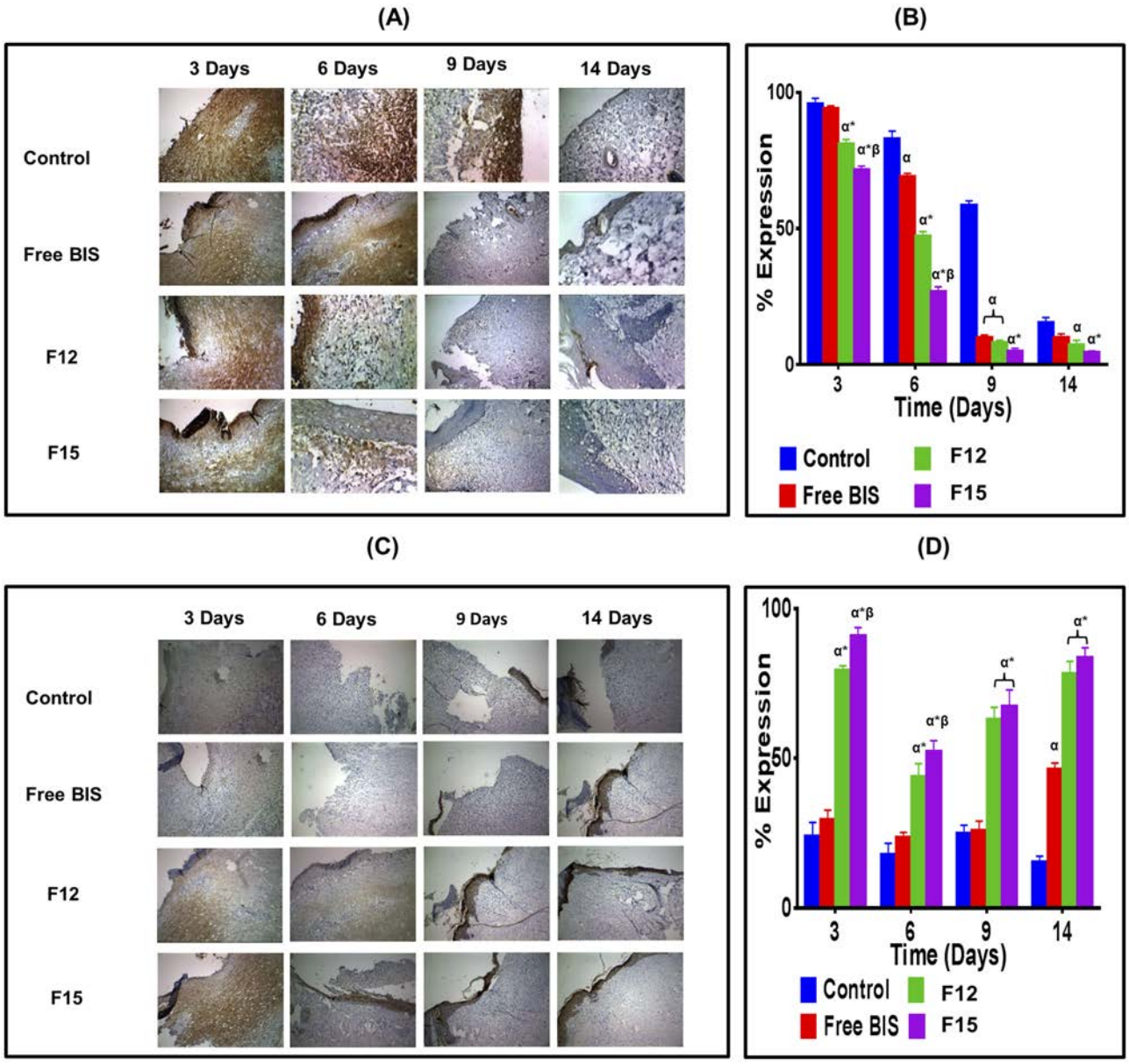

Figure 5 Immunohistochemical study of wound sections 3, 6, 9 and 14 days post-wounding of control, free BIS, F12 (blank 7% C-ZNFs), and F15 (50% BIS-loaded 7% C-ZNFs scaffolds)-treated groups. (**A**) representative immunohistochemical NF-κB staining (×10 magnification), (**B**) % expression of NF-κB, (**C**) representative immunohistochemical Cytokeratin AE1/AE3 staining (×10 magnification) and (**D**) % expression of Cytokeratin AE1/AE3. *(α P < 0.05 vs Control; *P < 0.05 vs Free BIS; β P < 0.05 vs F12(blank 7% C-ZNFs)).*

promising wound dressing that can accelerate wound healing and tissue regeneration.

Ethical conduct of research

The authors state that they have followed the principles outlined in the Declaration of Helsinki for all animal experimental investigations.

Acknowledgments

The authors have no relevant affiliations or financial involvement with any organization or entity with a financial interest, financial conflict with the subject matter or materials discussed in the manuscript. This includes employment, consultancies, honoraria, stock ownership or options, expert testimony, grants or patents received or pending, or royalties. No writing assistance was utilized in the production of this manuscript.

Disclosure

The authors report no conflicts of interest in this work.

References

1. Rajkumar RJ, Nadar MM, Selvakumar PM. Nanotechnology in wound healing- a review. *Glob J Nano*. 2017;3(1):55560–55565.
2. Saporito F, Sandri G, Bonferoni MC, et al. Essential oil-loaded lipid nanoparticles for wound healing. *Int J Nanomedicine*. 2017;13:175–186. doi:10.2147/IJN.S152529
3. Ma L, Gao C, Mao Z, et al. Collagen/chitosan porous scaffolds with improved biostability for skin tissue engineering. *Biomaterials*. 2003;24(26):4833–4841. doi:10.1016/s0142-9612(03)00374-0
4. Dhandayuthapani B, Poulose AC, Nagaoka Y, et al. Biomimetic smart nanocomposite: in vitro biological evaluation of zein electrospun fluorescent nanofiber encapsulated CdS quantum dots. *Biofabrication*. 2012;4(2):025008. doi:10.1088/1758-5082/4/2/025008
5. Li F, Chen Y, Liu S, et al. Size-controlled fabrication of zein nano/microparticles by modified anti-solvent precipitation with/without sodium caseinate. *Int J Nanomedicine*. 2017;12:8197. doi:10.2147/IJN.S143733
6. Podaralla S, Averineni R, Alqahtani M, Perumal O. Synthesis of novel biodegradable methoxy poly(ethylene glycol)-zein micelles for effective delivery of curcumin. *Mol Pharm*. 2012;9(9):2778–2786. doi:10.1021/mp2006455
7. Ashok P, Patricia H, Johan H, Ellen D, Krassimir V. Quercetin loaded biopolymeric colloidal particles prepared by simultaneous precipitation of quercetin with hydrophobic protein in aqueous medium. *Food Chem*. 2012;133(2):423–429. doi:10.1016/j.foodchem.2012.01.054
8. Zou T, Gu L. TPGS emulsified zein nanoparticles enhanced oral bioavailability of daidzin: in vitro characteristics and in vivo performance. *Mol Pharm*. 2013;10(5):2062–2070. doi:10.1021/mp400086n
9. El-Lakany SA, Elgindy NA, Helmy MW, Abu-Serie MM, Elzoghby AO. Lactoferrin-decorated vs PEGylated zein nanospheres for combined aromatase inhibitor and herbal therapy of breast cancer. *Expert Opin Drug Deliv*. 2018;15(9):835–850. doi:10.1080/17425247.2018.1505858
10. Elzoghby AO, El-Lakany SA, Helmy MW, Abu-Serie MM, Elgindy NA. Shell-crosslinked zein nanocapsules for oral codelivery of exemestane and resveratrol in breast cancer therapy. *Nanomedicine (Lond)*. 2017;12(24):2785–2805. doi:10.2217/nnm-2017-0247
11. Lai L, Guo H. Preparation of new 5-fluorouracil-loaded zein nanoparticles for liver targeting. *Int J Pharm*. 2011;404(1–2):317–323. doi:10.1016/j.ijpharm.2010.11.025
12. Torres-Giner S, Ocio MJ, Lagaron JM. Novel antimicrobial ultrathin structures of zein/chitosan blends obtained by electrospinning. *Carbohydr Polym*. 2009;77(2):261–266. doi:10.1016/j.carbpol.2008.12.035
13. Fan W, Jie W, Changsheng L, Brian ON, Ngothai Y. Fabrication and properties of porous scaffold of zein/PCL biocomposite for bone tissue engineering. *Compos Part B*. 2012;43(5):2192–2197. doi:10.1016/j.compositesb.2012.02.040
14. Selling GW, Woods KK, Sessa D, Biswas A. Electrospun zein fibers using glutaraldehyde as the crosslinking reagent: effect of time and temperature. *Macromol Chem Phys*. 2008;209(10):1003–1011. doi:10.1002/(ISSN)1521-3935
15. Jiang Q, Yang Y. Water-stable electrospun zein fibers for potential drug delivery. *J Biomat Sci-Polym E*. 2011;22(10):1393–1408.
16. Kharaghani D, Khan MQ, Yamamoto T, Soo Kim I. Antibacterial properties of in situ and surface functionalized impregnation of silver sulfadiazine in polyacrylonitrile nanofiber mats. *Int J Nanomed*. 2019;14:2693–2703. doi:10.2147/IJN.S197665
17. Huang W, Zou T, Li S, Jing J, Xia X, Liu X. Drug-loaded zein nanofibers prepared using a modified coaxial electrospinning process. *AAPS PharmSciTech*. 2013;14(2):675–681. doi:10.1208/s12249-013-9953-1
18. Marongiu L, Donini M, Bovi M, et al. The inclusion into PLGA nanoparticles enables α-bisabolol to efficiently inhibit the human dendritic cell pro-inflammatory activity. *J Nanopart Res*. 2014;16(8):2554. doi:10.1007/s11051-014-2554-4
19. Rocha NF, Rios ER, Carvalho AM, et al. Anti-nociceptive and anti-inflammatory activities of (-)-alpha-bisabolol in rodents. *Naunyn-Schmiedeberg's Arch Pharmacol*. 2011;384(6):525–533. doi:10.1007/s00210-011-0679-x
20. Kim S, Jung E, Kim JH, Park YH, Lee J, Park D. Inhibitory effects of (-)-alpha-bisabolol on LPS-induced inflammatory response in RAW264.7 macrophages. *Food Chem Toxicol*. 2011;49(10):2580–2585. doi:10.1016/j.fct.2011.06.076
21. Hotaling NA, Bharti K, Kriel H, Simon CG. DiameterJ: a validated open source nanofiber diameter measurement tool. *Biomaterials*. 2015;61:327–338. doi:10.1016/j.biomaterials.2015.05.015
22. Bonthagarala B, Swain S, Rao PV, Dasari V. Design and characterization of controlled release lornoxicam nanofibers by electrospinning technique. *IJABBR*. 2015;6(03):220–232.
23. Sathya S, Shanmuganathan B, Manirathinam G, Ruckmani K, Devi KP. α-bisabolol loaded solid lipid nanoparticles attenuates Aβ aggregation and protects neuro-2a cells from Aβ induced neurotoxicity. *J Mol Liq*. 2018;264:431–441. doi:10.1016/j.molliq.2018.05.075
24. Dash S, Murthy PN, Nath L, Chowdhury P. Kinetic modeling on drug release from controlled drug delivery systems. *Acta Pol Pharm*. 2010;67(3):217–223.
25. Almahdy O, El-Fakharany EM, El-Dabaa E, Ng TB, Redwan EM. Examination of the activity of camel milk casein against hepatitis C virus (genotype-4a) and its apoptotic potential in hepatoma and hela cell lines. *Hepat Mon*. 2011;11(9):724–730. doi:10.5812/kowsar.1735143X.722
26. Mosmann T. Rapid colorimetric assay for cellular growth and survival: application to proliferation and cytotoxicity assays. *J Immunol Methods*. 1983;65(1–2):55–63. doi:10.1016/0022-1759(83)90303-4
27. Preet R, Mohapatra P, Mohanty S, et al. Quinacrine has anticancer activity in breast cancer cells through inhibition of topoisomerase activity. *Int J Cancer*. 2012;130(7):1660–1670. doi:10.1002/ijc.26158
28. You C, Li Q, Wang X, et al. Silver nanoparticle loaded collagen/chitosan scaffolds promote wound healing via regulating fibroblast migration and macrophage activation. *Sci Rep*. 2017;7(1):10489. doi:10.1038/s41598-017-10481-0
29. Samy WM, Ghoneim AI, Elgindy NA. Novel microstructured sildenafil dosage forms as wound healing promoters. *Expert Opin Drug Deliv*. 2014;11(10):1525–1536. doi:10.1517/17425247.2014.929662
30. Hajiaghaalipour F, Kanthimathi MS, Abdulla MA, Sanusi J. The effect of camellia sinensis on wound healing potential in an animal model. *Evidence-based Complementary Altern Med*. 2013;2013:386734. doi:10.1155/2013/386734
31. Abramov Y, Golden B, Sullivan M, et al. Histologic characterization of vaginal vs. abdominal surgical wound healing in a rabbit model. *Wound Repair Regener*. 2007;15(1):80–86. doi:10.1111/j.1524-475X.2006.00188.x
32. Babitha S, Korrapati PS. Biodegradable zein–polydopamine polymeric scaffold impregnated with TiO2 nanoparticles for skin tissue engineering. *Biomed Mater*. 2017;12(5):055008. doi:10.1088/1748-605X/aa7d5a
33. Jiang H, Zhao P, Zhu K. Fabrication and characterization of zein-based nanofibrous scaffolds by an electrospinning method. *Macromol Biosci*. 2007;7(4):517–525. doi:10.1002/mabi.200600277
34. Deitzel JM, Kleinmeyer J, Harris D, Beck Tan NC. The effect of processing variables on the morphology of electrospun nanofibers and textiles. *Polymer*. 2001;42(1):261–272. doi:10.1016/S0032-3861(00)00250-0
35. Zargham S, Bazgir S, Tavakoli A, Rashidi AS, Damerchely R. The effect of flow rate on morphology and deposition area of electrospun nylon 6 nanofiber. *J Eng Fiber Fabr*. 2012;7(4):155892501200700414.
36. Doane DP, Seward LE. Measuring skewness: a forgotten statistic? *J Stat Educ*. 2011;19:2. doi:10.1080/10691898.2011.11889611

37. Torres-Giner S, Gimenez E, Lagarón JM. Characterization of the morphology and thermal properties of zein prolamine nanostructures obtained by electrospinning. *Food Hydrocoll*. 2008;22(4):601–614. doi:10.1016/j.foodhyd.2007.02.005
38. Reddy N, Li Y, Yang Y. Alkali-catalyzed low temperature wet cross-linking of plant proteins using carboxylic acids. *Biotechnol Prog*. 2009;25(1):139–146. doi:10.1002/btpr.86
39. Pillay V, Dott C, Choonara YE, et al. A review of the effect of processing variables on the fabrication of electrospun nanofibers for drug delivery applications. *J Nanomater*. 2013;22:1–22.
40. de Oliveira Mori CL, Dos Passos NA, Oliveira JE, et al. Electrospinning of zein/tannin bio-nanofibers. *Ind Crops Prod*. 2014;52:298–304. doi:10.1016/j.indcrop.2013.10.047
41. Lee Y-F, Sridewi N, Ramanathan S, Sudesh K. The Influence of electrospinning parameters and drug loading on polyhydroxyalkanoate (PHA) nanofibers for drug delivery. *Int J Biotech Wellness Ind*. 2017;4(4):103–113.
42. Khalil AA, Deraz SF, Elrahman SA, El-Fawal G. Enhancement of mechanical properties, microstructure, and antimicrobial activities of zein films cross-linked using succinic anhydride, eugenol, and citric Acid. *Prep Biochem Biotech*. 2015;45(6):551–567. doi:10.1080/10826068.2014.940967
43. Yao C, Li X, Song T. Electrospinning and crosslinking of zein nanofiber mats. *J Appl Polym Sci*. 2007;103(1):380–385. doi:10.1002/(ISSN)1097-4628
44. Jiang Q, Reddy N, Yang Y. Cytocompatible cross-linking of electrospun zein fibers for the development of water-stable tissue engineering scaffolds. *Acta Biomater*. 2010;6(10):4042–4051. doi:10.1016/j.actbio.2010.04.024
45. Sessa DJ, Mohamed A, Byars JA. Chemistry and physical properties of melt-processed and solution-cross-linked corn zein. *J Agr Food Chem*. 2008;56(16):7067–7075. doi:10.1021/jf800712k
46. Wu Y, Luo Y, Wang Q. Antioxidant and antimicrobial properties of essential oils encapsulated in zein nanoparticles prepared by liquid–liquid dispersion method. *LWT - Food Sci Tech*. 2012;48(2):283–290. doi:10.1016/j.lwt.2012.03.027
47. Garcia PS, Grossmann MVE, Yamashita F, Mali S, Dall'Antonia LH, Barreto WJ. Citric acid as multifunctional agent in blowing films of starch/PBAT. *Química Nova*. 2011;34:1507–1510. doi:10.1590/S0100-40422011000900005
48. Tavakolipour H, Bagheri L, Madadlou A. Pomegranate seed oil-loaded particles of the zein cross-linked with citric acid. *J Food Process Eng*. 2015;38(1):49–56. doi:10.1111/jfpe.12125
49. Souza F, Souza R, Moraes Â. Incorporation and release kinetics of alpha-bisabolol from PCL and chitosan/guar gum membranes. *Braz J Chem Eng*. 2016;33(3):453–467. doi:10.1590/0104-6632.20160333s20150083
50. Menzies KL, Jones L. The impact of contact angle on the biocompatibility of biomaterials. *Optometry Vision Sci*. 2010;87(6):387–399. doi:10.1097/OPX.0b013e3181da863e
51. Vogt L, Liverani L. Electrospun zein fibers incorporating Poly(glycerol sebacate) for soft tissue engineering. *Nanomaterials*. 2018;8(3):150.
52. Samy W, Elgindy N, El-Gowelli HM. Biopolymeric nifedipine powder for acceleration of wound healing. *Int J Pharm*. 2012;422(1–2):323–331.
53. Grip J, Engstad RE, Skjæveland I, et al. Beta-glucan-loaded nanofiber dressing improves wound healing in diabetic mice. *Eur J Pharm Sci*. 2018;121:269–280. doi:10.1016/j.ejps.2018.05.031
54. Jiang Q, Reddy N, Zhang S, Roscioli N, Yang Y. Water-stable electrospun collagen fibers from a non-toxic solvent and crosslinking system. *J Biomed Mater Res Part A*. 2013;101(5):1237–1247. doi:10.1002/jbm.a.34422
55. Cui H, Liu GL, Padua GW. Cell spreading and viability on zein films may be facilitated by transglutaminase. *Colloids Surf*. 2016;145:839–844. doi:10.1016/j.colsurfb.2016.05.048
56. Chirumbolo S. Alpha-bisabolol, not a matter for cancer therapy. Commentary: "research on the immunosuppressive activity of ingredients contained in sunscreens". *Front Pharmacol*. 2015;6(96). doi:10.3389/fphar.2015.00096
57. Wang H, Radjendirane V, Wary KK, Chakrabarty S. Transforming growth factor beta regulates cell-cell adhesion through extracellular matrix remodeling and activation of focal adhesion kinase in human colon carcinoma Moser cells. *Oncogene*. 2004;23(32):5558–5561. doi:10.1038/sj.onc.1207701
58. Dong J, Sun Q, Wang J. Basic study of corn protein, zein, as a biomaterial in tissue engineering, surface morphology and biocompatibility. *Biomaterials*. 2004;25(19):4691–4697. doi:10.1016/j.biomaterials.2003.10.084
59. Yeh C-J, Chen -C-C, Leu Y-L, Lin M-W, Chiu -M-M, Wang S-H. The effects of artocarpin on wound healing: in vitro and in vivo studies. *Sci Rep*. 2017;7(1):15599. doi:10.1038/s41598-017-15876-7
60. Mariggiò MA, Cassano A, Vinella A, et al. Enhancement of fibroblast proliferation, collagen biosynthesis and production of growth factors as a result of combining sodium hyaluronate and aminoacids. *Int J Immunopath Ph*. 2009;22(2):485–492. doi:10.1177/039463200902200225
61. Bezerra SB, Leal LKAM, Nogueira NAP, Campos AR. Bisabolol-induced gastroprotection against acute gastric lesions: role of prostaglandins, nitric oxide, and K+ATP channels. *J Med Food*. 2009;12(6):1403–1406. doi:10.1089/jmf.2008.0290
62. Girault A, Brochiero E. Evidence of K+ channel function in epithelial cell migration, proliferation, and repair. *M J Physiol Cell Physiol*. 2014;306(4):C307–C319. doi:10.1152/ajpcell.00226.2013
63. Eming SA, Martin P, Tomic-Canic M. Wound repair and regeneration: mechanisms, signaling, and translation. *Sci Transl Med*. 2014;6(265):265sr266. doi:10.1126/scitranslmed.3009337
64. Martin P, Leibovich SJ. Inflammatory cells during wound repair: the good, the bad and the ugly. *Trends Cell Biol*. 2005;15(11):599–607. doi:10.1016/j.tcb.2005.09.002
65. White ES, Mantovani AR. Inflammation, wound repair, and fibrosis: reassessing the spectrum of tissue injury and resolution. *J Pathol*. 2013;229(2):141–144. doi:10.1002/path.4126
66. Park DH, Kim SB, Lee JS, inventors; Biospecrum Inc, assignee. Compositions for improving skin conditions comprising alpha-bisabolol as an active ingredient. In: *Google Patents*. 2010. No.12/527,756.
67. Lawrence T. The nuclear factor NF-kappaB pathway in inflammation. *Cold Spring Harb Perspect Biol*. 2009;1(6):a001651–a001651. doi:10.1101/cshperspect.a001651
68. Watanabe S, Osumi M, Ohnishi T, Ichikawa E, Takahashi H. Changes in cytokeratin expression in epidermal keratinocytes during wound healing. *Histochem Cell Biol*. 1995;103(6):425–433.
69. Erwin E, Gunanti HE, Noviana D. Changes in histopathology and cytokeratin AE1/AE3 expression in skin graft with different time on Indonesian local cats. *Vet World*. 2017;10(6):662–666. doi:10.14202/vetworld.2017.662-666
70. Sabol F, Dancakova L, Gál P, et al. Immunohistological changes in skin wounds during the early periods of healing in a rat model. *Vet Med (Praha)*. 2012;157(2):77–82.